Opt Quant Electron
DOI 10.1007/s11082-008-9221-x

Design and optimization of a GaAs-based sub-7-μm quantum cascade laser based on multivalley Monte Carlo simulation

Xujiao Gao · Mithun D'Souza · Dan Botez · Irena Knezevic

Received: 28 August 2007 / Accepted: 20 May 2008

Abstract We present the design and optimization of a deep-well GaAs-based quantum cascade laser (QCL) emitting at 6.7 μm, the shortest wavelength in GaAs-based QCLs, using a multivalley Monte Carlo simulation. Simulation results provide direct insights into optimizing the layer sequence design. The optimized structure exhibits sufficient gain for lasing at both 77 and 300 K. The calculated threshold-current densities are 5 kA/cm^2 at 77 K and 14 kA/cm^2 at 300 K.

Keywords Multivalley Monte Carlo simulation · Quantum cascade lasers · X-valley leakage

1 Introduction

Quantum cascade lasers (QCLs) (Faist et al. 1994; Page et al. 2001) are electrically pumped unipolar coherent mid- to far-infrared light sources, where an electron cascades down the energy level staircase in multi-quantum-well structures and emits multiple photons. QCLs are generally fabricated on either InP (Faist et al. 1994) or GaAs (Page et al. 2001) substrates. Among GaAs-based mid-infrared (mid-IR) QCLs, the 9.4 μm GaAs QCL by Page et al. (2001) has shown the best device performance so far, i.e., pulsed room-temperature operation and continuous-wave operation up to 150 K (Page et al. 2004). However, this type of QCLs shows a short wavelength limit of 8 μm, due to the intervalley carrier loss when the upper lasing level becomes aligned with the lowest X-valley state of the injection barrier (Wilson et al. 2002).

In this paper, we present the design and optimization of a 6.7 μm $In_{0.1}Ga_{0.9}As/GaAs/Al_{0.45}Ga_{0.55}As$ QCL structure, the shortest wavelength to date in GaAs-based QCLs. Transport properties of three layer sequence designs are simulated utilizing a Monte Carlo simulator (Gao et al. 2006, 2007a) with both Γ- and X-valley transport included. Simulation results

X. Gao · M. D'Souza · D. Botez · I. Knezevic (✉)
Department of Electrical and Computer Engineering, University of Wisconsin–Madison,
1415 Engineering Drive, Madison, WI 53706, USA
e-mail: knezevic@engr.wisc.edu

from the first two designs directly provide physical insights into obtaining an optimized design. The optimized structure is predicted to have threshold-current densities of 5 kA/cm^2 at 77 K and 14 kA/cm^2 at 300 K, similar to the experimental values obtained for the 9.4 µm GaAs QCL (Page et al. 2001).

2 Proposed QCL structure

The proposed QCL structure utilizes $Al_{0.45}Ga_{0.55}As$ in the barriers, GaAs in the injector wells, and strained $In_{0.1}Ga_{0.9}As$ in the two wide active-region quantum wells. The novelty of this structure is that using strained $In_{0.1}Ga_{0.9}As$ deep wells in the active region enables one to achieve lasing at 6.7 µm, below the 8 µm limit (Wilson et al. 2002). To partly compensate the compressive strain in the active region, one tensilely strained $GaAs_{0.6}P_{0.4}$ layer is added just before the injection barrier within each stage. Three structures (referred to as A, B, C) with different thickness of the layer sequence were designed and simulated. They were all designed to lase around 6.7 µm. The layers' thickness of structure C was optimized based on simulation results from the first two structures, as shown in the next section.

Figure 1 shows the calculated conduction band profile and the moduli squared of the relevant Γ- and X-valley wave functions in two adjacent stages for the optimized structure C (Gao et al. 2007b). At the field $F = 55$ kV/cm (close to the estimated threshold field of 58 kV/cm) and $T = 77$ K, the calculated lifetime due to electron-longitudinal optical (electron-LO) phonon interaction is $\tau_3 = 1.5$ ps for level 3 and $\tau_2 \approx \tau_{21} = 0.3$ ps for level 2. The dipole matrix element $\langle z_{32} \rangle$ is 1.5 nm. The lifetimes and matrix element are comparable to those of the 9.4 µm GaAs QCL ($\tau_3 = 1.4$ ps, $\tau_2 = 0.3$ ps, and $\langle z_{32} \rangle = 1.7$ nm) (Page et al. 2001).

3 Multivalley Monte Carlo simulation

The multivalley Monte Carlo simulator (Gao et al. 2006, 2007a) that we have recently developed is a suitable approach for transport simulation of mid-IR QCLs. It not only captures the correct steady-state electron dynamics in QCL devices, but also provides physical insight for design optimization. In this simulator, Γ-valley states are calculated using the $\mathbf{k} \bullet \mathbf{p}$ method within the envelope function approximation, while the X-valley states are obtained by solving the effective mass equation (Gao et al. 2007a). All the relevant scattering mechanisms are included: electron-LO, electron–electron, and intervalley scattering processes within the same stage and between adjacent stages. The Monte Carlo simulation yields macroscopic quantities of interest, such as the current density J and subband electron density at each electric field. The modal gain G_m can be calculated as a function of the current density, and a realistic threshold current density is then determined (Gao et al. 2007b).

The inclusion of the X-valley transport in the simulation allows for quantifying the leakage current through the X valleys. It was shown (Gao et al. 2006, 2007a) that the X-valley leakage occurs due to the strong coupling between the Γ-continuum (Γ_c) states (levels 4 and 5 in Fig. 1) and the X-states in the same stage, as seen in Fig. 1b; the Γ_c-states are populated through the scattering from the previous-stage injector miniband states. In order to minimize the X-valley leakage for improved population inversion and reduced current density, the wave function overlap of the injector states with the next-stage Γ_c-states needs to be minimized. With this design strategy in mind, we varied the thickness of the layer sequence of the proposed structure and performed the Monte Carlo simulation. The goal was to obtain a particular design of the layer thickness so that the resulting QCL would achieve sufficient

Journal: 11082 MS: OQEL651 CMS: 11082_2008_9221_Article TYPESET DISK LE CP Disp.:2008/6/2 Pages: 6 Layout: Small

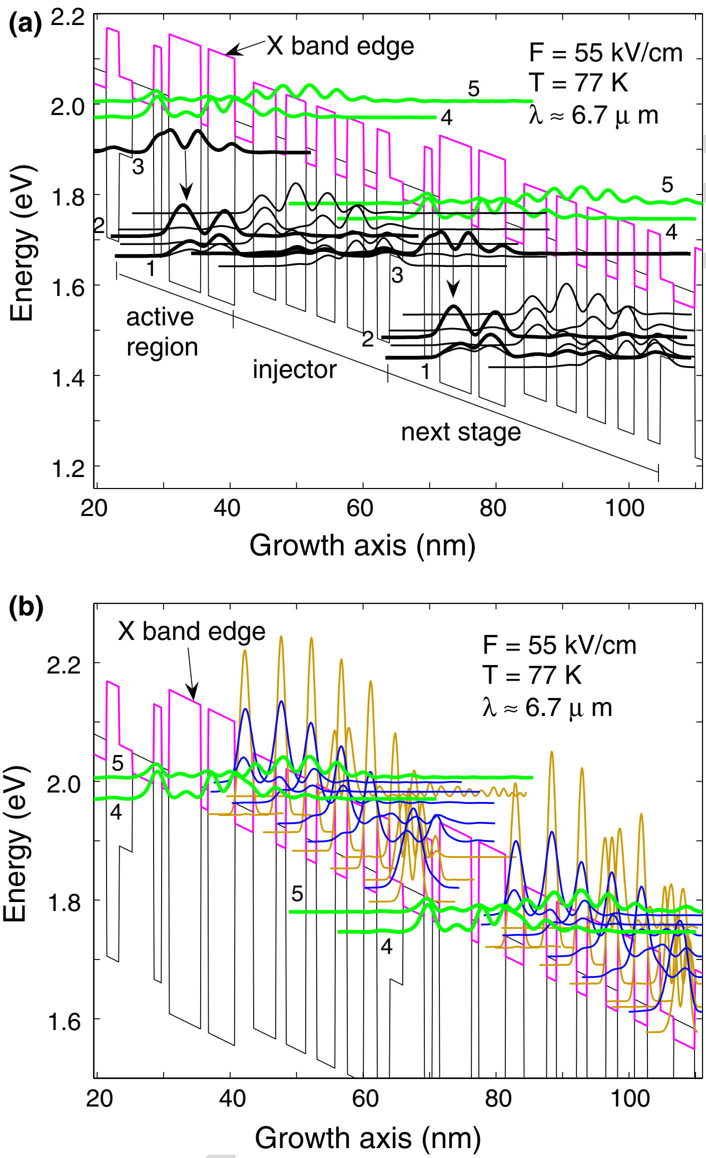

Fig. 1 Calculated conduction band profile and the moduli squared of the relevant Γ- and X-valley wave functions in two adjacent stages for the optimized structure C. (**a**) The bold black lines denote the active lasing levels (3—upper, 2—lower, 1—ground). The thin black lines are the injector miniband states, and the bold green lines are the Γ-continuum states (levels 4 and 5). The vertical arrow denotes the lasing transition. The layer sequence in one stage (in Angstrom) starting from the $GaAs_{0.6}P_{0.4}$ barrier on the left is ***20***, **32**, 12, **11**, {48}, **11**, {40}, **28**, 34, **15**, 30, <u>**16**</u>, <u>28</u>, <u>**18**</u>, <u>25</u>, **20**, 19. (The layer sequence of structure A is ***20***, **28**, 12, **11**, {48}, **11**, {40}, **28**, 38, **13**, 34, <u>**14**</u>, <u>25</u>, <u>**16**</u>, <u>22</u>, **17**, 17, and structure B ***20***, **28**, 12, **11**, {48}, **11**, {40}, **28**, 38, **13**, 30, <u>**14**</u>, <u>30</u>, <u>**16**</u>, <u>27</u>, **17**, 25.) The bold italic script denotes the $GaAs_{0.6}P_{0.4}$ barrier, the bold script the $Al_{0.45}Ga_{0.55}As$ barriers, the normal script the GaAs wells, and the values in curly brackets indicate the $In_{0.1}Ga_{0.9}As$ wells. The underlined layers are n-type doped with a sheet doping density of $N_s = 3.8 \times 10^{11}\ \mathrm{cm}^{-2}$. (**b**) The thin blue lines are the (degenerate) X_x- and X_y-states and the yellow ones are the X_z-states

gain for lasing at both 77 K and 300 K. Simulation results enable us to identify whether a design meets the goal and find out the issues with the design if it does not. This design-simulation process is repeated until an optimized layer sequence is obtained.

The electric field vs current density is shown in Fig. 2 for the three structures A, B, and C. The current densities include the leakage currents through the next-stage Γ_c-states and the X-valley states (Gao et al. 2007a). Figure 3 compares the modal gain vs current density for

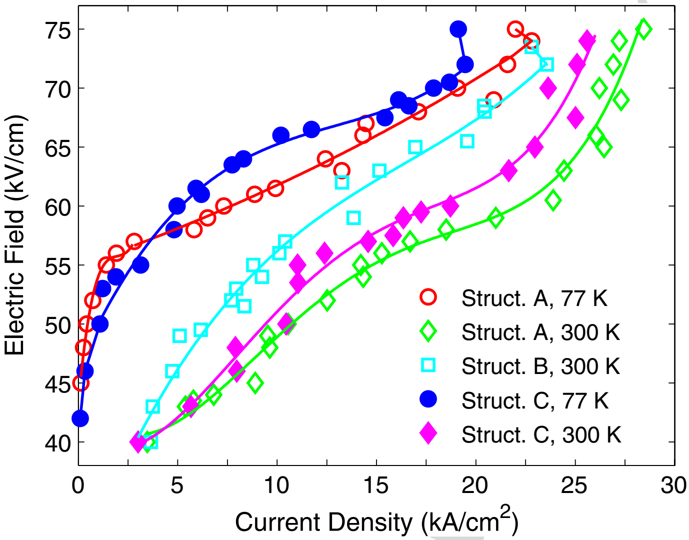

Fig. 2 Electric field versus current density at the lattice temperatures of 77 K and 300 K for the three structures A, B, and C. The solid lines are guides for the eyes

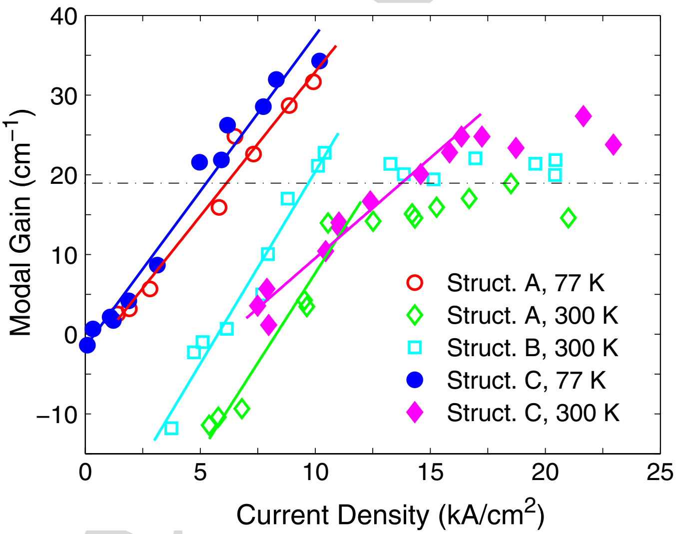

Fig. 3 Modal gain versus current density at the 77 and 300 K lattice temperatures for the three structures A, B, and C. The horizontal dash-dot line indicates the calculated total losses $\alpha_w + \alpha_m$. The solid lines are linear least-square fits to the data points in the region of relatively low current densities, which intersect the loss line giving the threshold current density Jth

Journal: 11082 MS: OQEL651 CMS: 11082_2008_9221_Article TYPESET DISK LE CP Disp.:2008/6/2 Pages: 6 Layout: Small

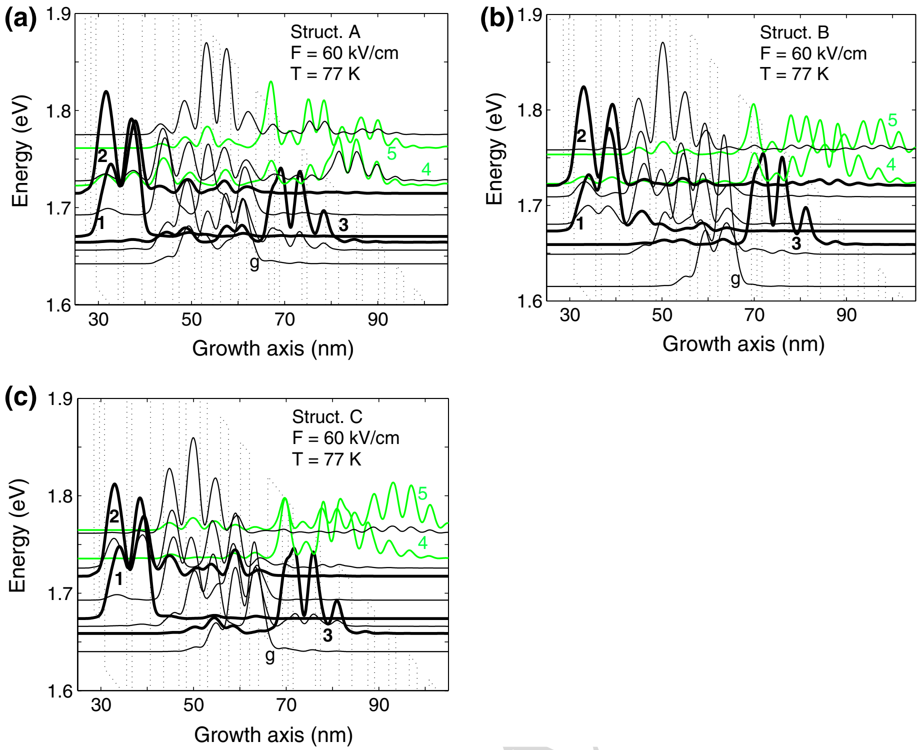

Fig. 4 Relevant wave function moduli squared, illustrating the coupling of the injector miniband states with the next-stage Γ_c-states. Notation is the same as in Fig. 1

the three structures. The total losses are calculated to be $19\,\mathrm{cm}^{-1}$ ($\alpha_w = 15\,\mathrm{cm}^{-1}$, waveguide loss, plus $\alpha_m = 4\,\mathrm{cm}^{-1}$, mirror loss) based on an improved waveguide design (Gao et al. 2007b). The initial design (structure A) shows sufficient gain at 77 K, but at 300 K the gain saturates below the total loss line, which is because the strong coupling of the injector states with the next-stage Γ_c-states, as shown in Fig. 4a, results in large carrier loss to the X-valleys, largely reducing the population inversion. To decrease this detrimental coupling, the injector well thickness in structure B was increased in order to bring down the injector top state and shift its wave function maximum away from the continuum (Fig. 4b). As a result, structure B does demonstrate enough gain at 300 K. The tradeoff is that the modal gain at 77 K was inadequate, since the next-stage upper lasing level is more weakly coupled to the injector ground state (level g) and far above in energy level (Fig. 4b) leading to electron accumulation in the injector ground state. In contrast at 300 K, the electrons distribute among all the Γ-subbands due to active phonons, and thus lasing can occur. Identification of issues with structures A and B directly helps the optimization of structure C. The layer sequence of structure C is designed such that not only the coupling between the injector states and next-stage Γ_c-states is reduced, but also the upper lasing level has good wave function overlap and small energy difference with the injector ground state as seen in Fig. 4c. The optimized structure C shows a threshold-current density Jth of $5\,\mathrm{kA/cm}^2$ at 77 K and $14\,\mathrm{kA/cm}^2$ at 300 K (structure B has $J\mathrm{th} = 9.5\,\mathrm{kA/cm}^2$ at 300 K due to the smaller currents in Fig. 2 and higher $\langle z_{32}\rangle = 1.6\,\mathrm{nm}$.), close to those for the 9.4 μm GaAs QCL ($J\mathrm{th} = 4\,\mathrm{kA/cm}^2$ at 77 K and $16.7\,\mathrm{kA/cm}^2$ at 300 K) (Page et al. 2001).

Journal: 11082 MS: OQEL651 CMS: 11082_2008_9221_Article TYPESET DISK LE CP Disp.:2008/6/2 Pages: 6 Layout: Small

4 Conclusion

Multivalley Monte Carlo simulations have been performed to optimize the design of a deep-well QCL structure that utilizes the $In_{0.1}Ga_{0.9}As/GaAs/\ Al_{0.45}Ga_{0.55}As$ materials system and emits at 6.7 µm. The unique inclusion of both Γ- and X-valley transport allows for identifying the issues associated with a particular design. Results from the first two designs play a direct and important role in obtaining the optimized layer sequence design, which shows sufficient gain for both 77 K and room-temperature lasing. The threshold-current densities are calculated to be 5 kA/cm^2 at 77 K and 14 kA/cm^2 at 300 K.

References

Faist, J., Capasso, F., Sivco, D.L., Sirtori, C., Hutchinson, A.L., Cho, A.Y.: Quantum cascade laser. Science **264**, 553–556 (1994)

Gao, X., Botez, D., Knezevic, I.: X-valley leakage in GaAs/AlGaAs quantum cascade lasers. Appl. Phys. Lett. **89**, 191119 (2006)

Gao, X., Botez, D., Knezevic, I.: J. Appl. Phys. **101**, 063101 (2007a)

Gao, X., D'Souza, M., Botez, D., Knezevic, I.: J. Appl. Phys. (submitted) (2007b)

Page, H., Becker, C., Robertson, A., Glastre, G., Ortiz, V., Sirtori, C.: 300 K operation of a GaAs-based quantum-cascade laser at 9 µm. Appl. Phys. Lett. **78**, 3529–3531 (2001)

Page, H., Dhillon, S., Calligaro, M., Becker, C., Ortiz, V., Sirtori, C.: IEEE J. Quantum Electron. **40**, 665 (2004)

Wilson, L.R., Carde, D.A., Cockburn, J.W., Green, R.P., Revin, D.G., Steer, M.J., Hopkinson, M., Hill, G., Airey, R.: Intervalley scattering in GaAs–AlAs quantum cascade lasers. Appl. Phys. Lett. **81**, 1378–1380 (2002)